**ORIGINAL ARTICLE**

# An integrated hydrogeological approach to evaluate the leakage potential from a complex and fractured karst aquifer, example of Abolabbas Dam (Iran)

Rouhollah Adinehvand[1] · Ezzat Raeisi[1] · Andreas Hartmann[2,3]

## Abstract

The design and construction of dams are risky in karst regions with active tectonic settings and strong heterogeneity due to their leakage potential. Hydrogeological characterization by karst-specific methods can be used to reduce the risk of improper dam construction. Numerous karstic dams have been constructed in the world in simple tectonic settings. In this study, a combination of geological and hydrogeological investigations is used with extensive data collection to evaluate the leakage potential of the Abolabbas Dam construction project at the Malagha karst aquifer, a tectonized highland karst region in the southwest of Iran. Two thrust faults which bounded the Malagha karst aquifer (overthrusting) caused extensive crushed zones, continuous lengths with high permeabilities in most of the boreholes, extensive open joints, and small-size solution cavities. The results of artificial tracer tests imply that the flow regime is diffuse. The flat water table, diffuse flow regime, extensive crushed zones, and continuous high-permeabilities most probably imply that the groundwater flows through an extensive network of joints without main conduits to drain the system. Despite a diffuse flow regime, an extensive grout curtain both in length and depth is required to prevent leakage because the loose materials of the crushed zones will be washed out without it under high hydraulic gradients after dam impoundment. The impermeable formation is too deep due to overthrusting. Therefore, a huge leakage may occur under the hanging grout curtain. The results allow a clearer understanding of the location and properties of fracture zones, erodible materials, high permeability zones, groundwater flow regime, and zones of preferential flow which are essential for reducing the failure of dam construction in such environments. Overall, it is demonstrated that integrating different complementary methods can help to minimize the uncertainties inherent in engineering problems in similar karst scarce-data regions.

**Keywords** Fractured karst aquifers · Diffuse flow · Leakage potential · Iran

## Introduction

The highly heterogeneous nature of karst aquifers (Bakalowicz 2005; Hartmann et al. 2014a; Hartmann and Baker 2017) makes them challenging environments for the design and development of engineering projects including dams

and reservoirs (Milanovic 2004; Gutiérrez et al. 2014; Parise et al. 2015). Numerous studies have been done on the leakage problems of karstic dam sites throughout the world (Turkmen et al. 2002; Unal et al. 2007; Uromeihy and Barzegari 2007; De Waele 2008; for a full review see, Bedmar and Araguas 2002; Milanovic 2004). In many cases, leakage has occurred immediately after the first filling (Milanovic 2014). The causes of such leakage can be classified into one or more of the following ways:

(a) the grout curtain is not connected to the impermeable layers. Therefore, leakage may occur below the hanging grout curtain, or from one or both of the abutments. Some examples are Bear Creek Dam (Bruce 2013), Keban Dam (Bozovic et al. 1981; Milanovic 2004), Canelles Dam (Milanovic 2004), and Mousol Dam (Sissakian et al. 2014). (b) Flow through the grout curtain due to unplugged

✉ Rouhollah Adinehvand
   radinehvand66@yahoo.com

1 Department of Earth Sciences, College of Sciences, Shiraz University, Shiraz, Fars Province 146713565, Iran

2 Chair of Hydrological Modeling and Water Resources, University of Freiburg, Freiburg, Germany

3 Department of Civil Engineering, University of Bristol, Bristol, UK

conduits, fault zones, and lack of grouting or cement mixture. (c) The wash-out of the soils and unconsolidated materials inside the joints and fractures due to high water pressure especially in dams with a high height. For example, Mujib Dam (Wiesner and Ewert 2013) and Great Falls Reservoir (Milanovic 2004). (d) Water leakage from the dam reservoir far from the dam foundation. For instance, Bogovina reservoir (Milanovic et al. 2010), Busko Blato reservoir (Milanovic 2004), and Anchor Dam (Jarvis 2003). (e) A combination of the above items. For instance, the Capljina Power Plant Reservoir (Milanovic 2004) and Anchor Dam (Jarvis 2003).

Systematic hydrogeological observations are needed during the design and construction stages which have to be integrated with the geotechnical basis for design (Merrit 1995). Successful solutions require serious and complex geological, hydrogeological, and geotechnical studies with the cooperation of scientists and engineers (Milanovic 2004).

Karst outcrops represent 11% of Iran's total land surface but their fraction increases to 21% in the southwest of Iran (Nassery 1991; Raeisi and Kowsar 1997). Numerous dams have been built on karstic sites and a few of them have leakage problems (Uromeihy 2000; Milanovic 2004; Ghobadi et al. 2005; Mohammadi et al. 2006; Mozafari and Raeisi 2015, 2017). The Abolabbas Dam is planned to be constructed on the Malagha karst aquifer at the tectonically active High Zagros Zone, inside the Malagha Gorge. The characterization of the Malagha karst aquifer is special and unique because most dams in Iran have been constructed in Zagros Simply Folded Belt or High Zagros. Different to those regions, Abolabbas Dam is located in a rough topography between two thrust faults in an active tectonized region and on an overturned limb of an anticline with repeated strata. The aquifer has an alluvial-like behavior and the faults act as a barrier, directing the groundwater flow parallel to the fault strike through a damage zone with extensive fractures, crushed zones, and minor faults (Adinehvand and Raeisi 2018). Therefore, it is expected that the hydrogeology of an active tectonized region is not similar to that of the Zagros Simply Folded Belt which is characterized by spectacular 'whaleback' shape anticlines (Blanc et al. 2003) and general flow direction parallel to the fold axis (Ashjari and Raeisi 2006). The results of a semi-distributed karst model with a step-wise simulation approach showed a huge leakage potential and a diffuse flow system (Adinehvand et al. 2017). In the dam site, the large number of the boreholes, dye tracings, stable isotopes, water balance, geological logs, water table configuration, and joint studies provide a good opportunity to study the relationship between the highly tectonized karst aquifer and the leakage potential of the dam site.

The objective of this study was to investigate the main characteristics of the highly tectonized Malagha karst aquifer and the integration of the detailed hydrogeological

properties such as permeabilities, open joints, fracture and crushed zones, wash-outs and vuggy zones, water table configuration, as well as stable isotopes, dye tracer tests, and the proposed grout curtain layout to estimate the leakage potential from the Abolabbas Dam site.

## Geological and hydrogeological setting

The study area has a semi-arid climate with the mean annual precipitation, evaporation, and temperature of 622 mm, 1457 mm, and 21 °C, respectively (Mahab Ghodss Consulting Engineers 2004). Precipitation typically occurs from November to May mostly in the form of rain and rarely snowfall (Zarei et al. 2014). The study area is located at the beginning of the High Zagros Zone in the southwest of Iran (James and Wynd 1965; Stocklin 1968; Falcon 1974; Berberian and King 1981; Berberian 1995; Alavi 2004; McQuarrie 2004; Talebian and Jackson 2004). The geological formations in decreasing order of age are Surmeh Limestone, Fahliyan-Dariyan Limestone, Ilam-Sarvak Limestone and marly limestone, Pabdeh-Gurpi marl, Asmari Limestone, Gachsaran marl, gypsum and salt, Aghajari marls and sandstones, and Bakhtiari conglomerate (Fig. 1a).

The main geological structures are the Chidan, Robat, and Malagha Anticlines with a NW–SE strike (Fig. 1a, b). In the western parts, some springs in the northern and southern limbs of the anticline discharge the karst groundwater (Fig. 1a). Robat Anticline is a small subsurface asymmetric anticline downstream of the Malagha thrust fault (Fig. 1b). The local Robat Aquifer (RA) is a limited exposed area formed in the Asmari Limestone of the northern limb of the Robat Anticline (Fig. 2). Two main reverse faults (Qale-Tol and Malagha) overturned the southern limb of the Malagha Anticline such that the connection of the Asmari Limestone of the northern and southern limbs has been disrupted. The Asmari Limestone of the southern overturned limb of the Malagha Anticline formed the Malagha Aquifer. The Malagha Aquifer is bounded by the Pabdeh-Gurpi Formations in the north, the Gachsaran Formation in the south, the anticline plunge in the east, and the Qale-Tol alluvial plain in the west (Fig. 1a). The Abolabbas River cuts through the Malagha Aquifer creating a vertical narrow gorge (the Malagha Gorge). The water level in the aquifer is about 60–70 m below the Abolabbas River bed at the dam site. The Abolabbas River seeps into the Malagha Aquifer along the Malagha Gorge with an average rate of 83 l/s (Adinehvand 2017).

The parts of the Malagha Aquifer around the dam site are named Dam-site Malagha Aquifer (DMA) in the following. It is bounded by the Pabdeh-Gurpi Formations in the north, Robat Aquifer (RA) in the south, and the boreholes in the east and west (Fig. 2). The boundary between the DMA and RA is the impermeable core of the Qale-Tol thrust fault
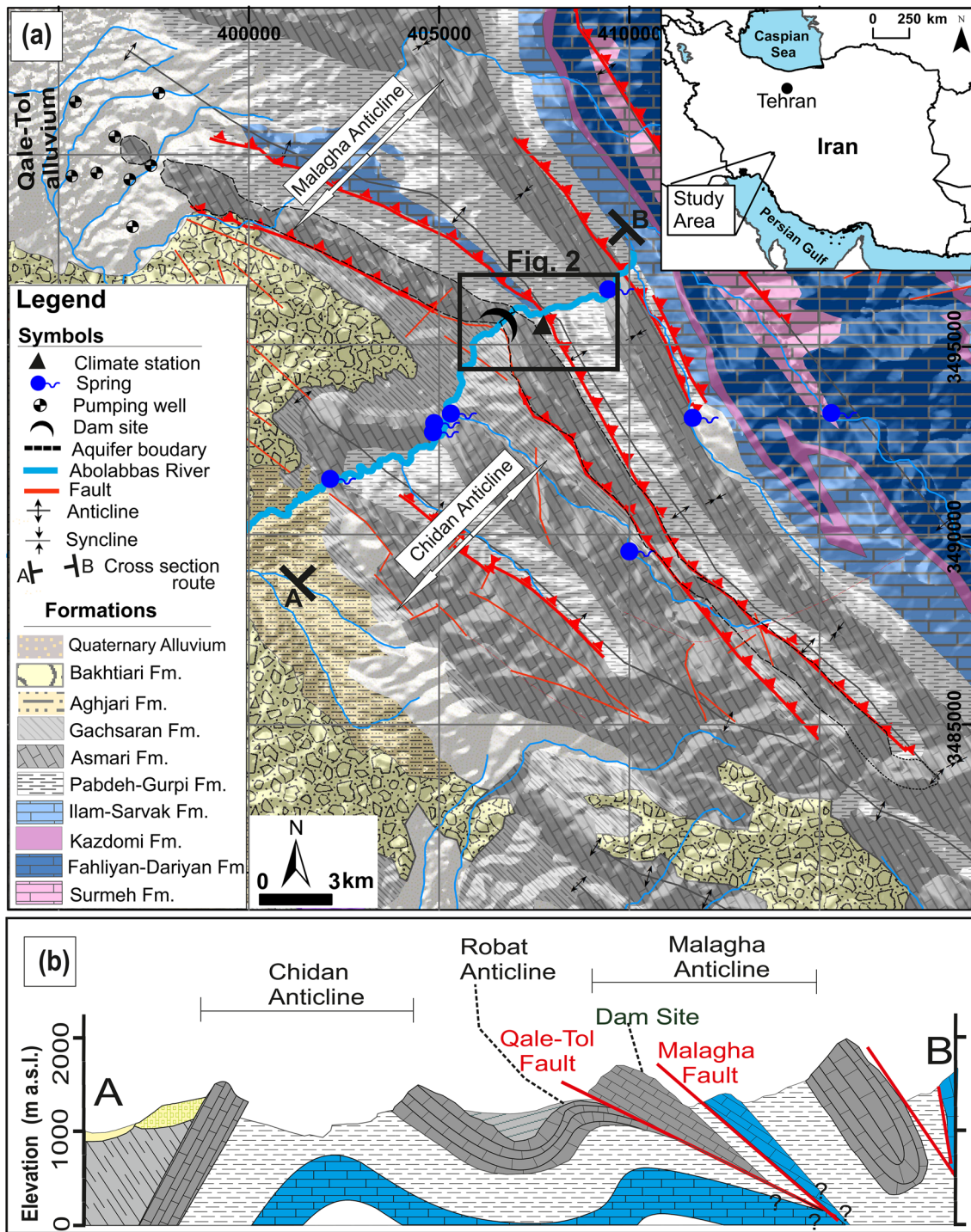
**Fig. 1** The geological map (**a**) and the cross-section (**b**) of the study area

(Adinehvand and Raeisi 2018). The Abolabbas Dam will be constructed on the Asmari Limestone of the southern overturned limb of the Malagha Anticline inside the Malagha Gorge (Figs. 1b, 2). The Asmari Limestone is classified into lower (As1), middle (As2), and upper (As3) units in decreasing order of age based on lithological characteristics

(Mahab Ghodss Consulting Engineers 2012) (Fig. 3a, b). The thicknesses of these three units are 110 m, 80 m, and 150 m, respectively. The As1 Unit underlies the Pabdeh-Gurpi marls (Fig. 3b). The As1 Unit consists of thick to massive limestone with intensive fractures and dissolution along the joints and bedding planes. Based on lithology, the
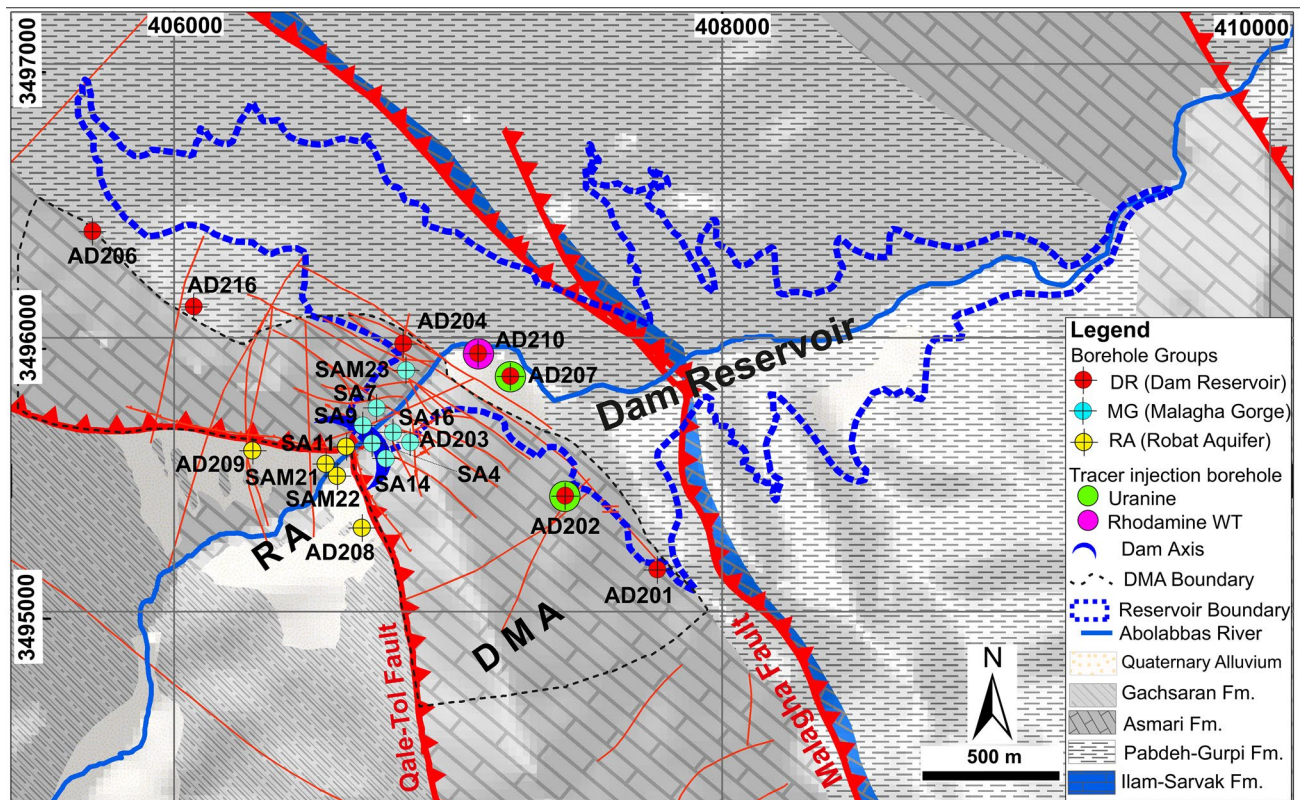
**Fig. 2** The geological map of the dam site area and the location of the dam reservoir, the Malagha and Qale-Tol faults, and the RA and DMA aquifers

As2 Unit is classified into three subunits consisting of thin to medium-bedded limestone with interbeds of marly limestone (As2-a), marly limestone to marlstone (As2-b), and thin to medium-bedded crystalline limestone with interbeds of marls and sandy limestones (As2-c) (Fig. 3b). The As3 Unit consists of thin to thick-bedded and massive limestone with dissolution along the bedding planes and cavities on the exposed surface along the Malagha Gorge (Fig. 3b).

## Materials and methods

### Site description

With a reservoir capacity of 113.4 $Mm^3$, the Abolabbas Dam is a double-arch dam with a height of 138 m above the foundation. It is located inside the Malagha Gorge at the southern flank of the Malagha Anticline (Fig. 1b). The reservoir normal water level is 1153 m above sea level (a.s.l.) (Majd 2011). The purposes of its construction are agriculture, hydroelectric power generation, and flood control. Parts of the reservoir and the abutments of the Abolabbas Dam are in direct contact with the karstified Asmari Limestone (Adine-hvand and Raeisi 2018) which has produced concerns about

water leakage after its construction. A detailed geology map, stable isotopes $^{18}O$ and $^2H$, river seepage, precipitation, and tracer tests were used to study the aquifer recharge, flow path, and flow regime of the Malagha karst aquifer (Adine-hvand and Raeisi 2018). In addition, the hydrogeological properties derived by measuring the permeability, fracture zones, open joints, core washes, and solution cavities in the borehole logs in an integrated approach were used in the characterization of the system to ensure a reliable grout curtain design and to minimize dam construction failure.

### Estimation of the hydrogeological properties

The geology maps of the study area with a 1:100,000 scale were obtained from the National Iranian Oil Company (1970) and the Geological Survey of Iran (1999). The permeability (in lugeon), fracture zones, open joints, core wash, rod falls, and vuggy zones were measured in all the borehole logs. The depths of the boreholes varied ranging from 85 to 330 m. The permeability was measured in lugeon at 5-m intervals using a double packer test. Fracture zones, core washes, and rod fall lengths were derived from the borehole log data. The number of the open joints per 5-m intervals and vuggy zones was also obtained from the borehole log
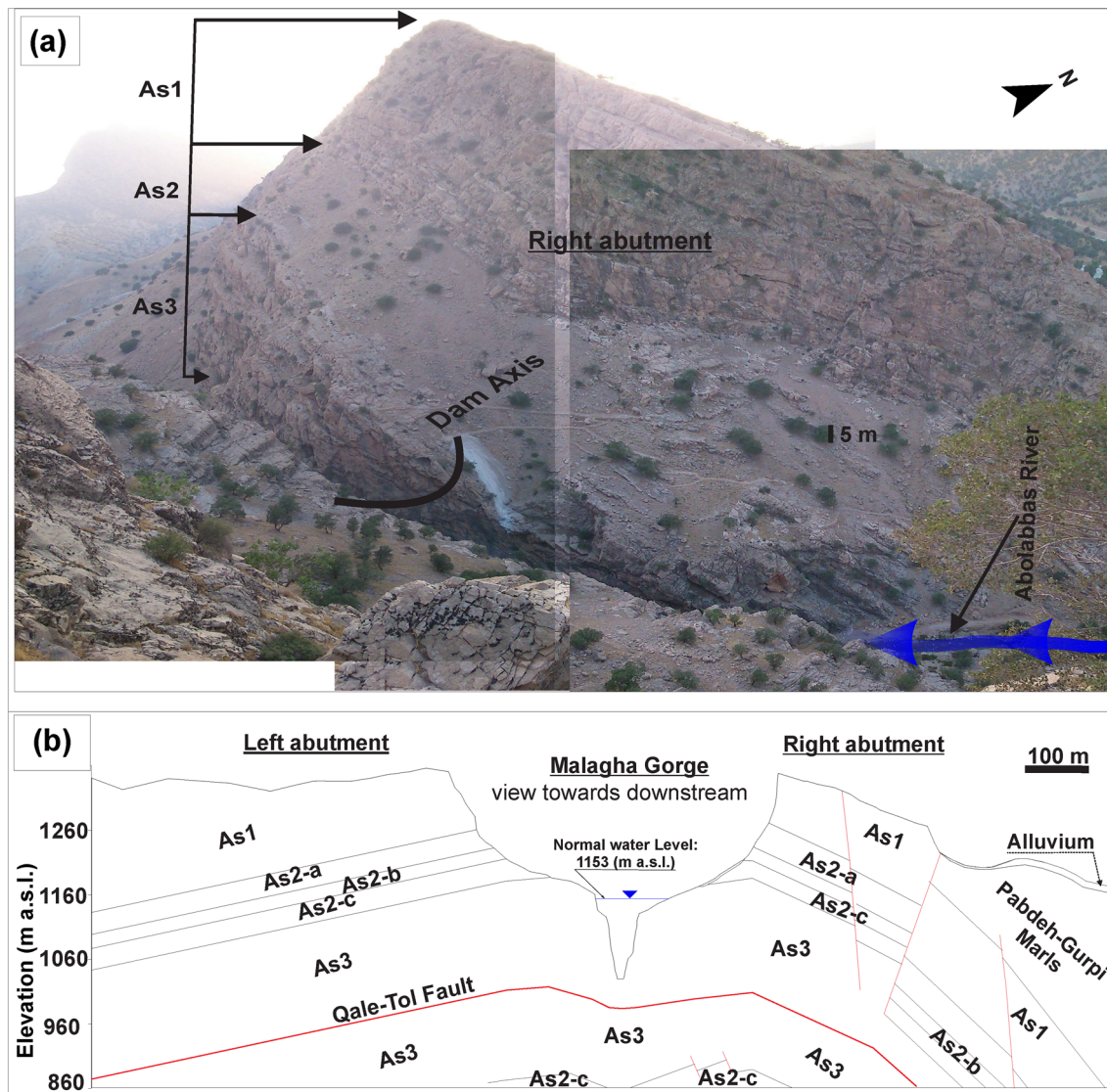
**Fig. 3** Abolabbas dam site and Malagha Gorge; **a** view of Malagha Gorge, from the left abutment towards the right one; **b** the geological cross-section across along dam axis (As2-b consists of 21 m of marly layers)

data. The recharge to the karst aquifer was assessed using a simple water balance method (Adinehvand and Raeisi 2018). The recharge coefficient was assumed to be 50% which is a typical value for the Mediterranean karst regions and the southwest of Iran (Rahnemaaie 1994; Hartmann et al. 2014b, 2015).

## Analysis of the spatial distribution of water table levels

The water table levels in the boreholes of the Malagha Aquifer and the Qale-Tol alluvial aquifer were measured several times during the study period (2010–2015). The water table level time series were analyzed to determine the fluctuations of the water table level in the karst aquifer and

the hydraulic connection between the river and karst groundwater through karst passages and numerous joints and fractures. The Abolabbas River flow rate at the Abolabbas Dam site was measured by the Khuzestan Regional Water and Power Authority (1994–2014). The seepage of the Abolabbas River at the Malagha Gorge was calculated by measuring the flow rate using a propeller-type water current meter at the entrance and exit of the Malagha Gorge (Adinehvand and Raeisi 2018).

## Artificial dye tracer tests

Tracer tests were conducted in order to characterize the groundwater flow and transport properties within the fracture and joint network of the Malagha Aquifer. Tracer tests

have been used to provide indispensable information on karst groundwater flow direction and pathways, to determine the flow velocities using the tracer travel time, and to define the type of flow by the shape of the breakthrough curves (Goldscheider 2005a; Mudarra et al. 2014). Using fluorescent dyes (uranine and rhodamine WT), three dye tracer tests were conducted in the Malagha Aquifer. In the first (in September 2010 and during the low water table period) and second (in June 2014 and during the high water table period) dye tracer tests, 15 kg and 40 kg of uranine (from MERK) were injected into boreholes AD-207 and AD-202, respectively (Fig. 2). In the first and second dye tracer tests, freshwater with several interruption periods and the discharge rates of about 0.5–1.0 l/s and 5–6 l/s was injected along with the dye into boreholes AD-207 and AD-202, respectively. In the third test, 86 L of rhodamine WT (from TURNER) were injected into borehole AD-210 in June 2014. The boreholes AD-207, AD-202, and AD-210 have high permeabilities below the water table level (20, 20, and 10 m, respectively, with the lugeon of 100). Freshwater with a discharge rate of about 2.5 l/s along with the dye was injected into borehole AD-210 with several interruption periods. The sampling points were 21 boreholes in the Malagha Aquifer and Robat Aquifer, 10 exploiting wells in the Qale-Tol alluvial aquifer, nine river sections along the Abolabbas River, and 12 springs of the Chidan Anticline. The sampling intervals which gradually increased were hourly on the first day for the near sampling points and daily for the faraway areas. In addition, charcoal bags were placed in the springs and river sections. The dye concentration was measured at the Department of Earth Sciences of Shiraz using a SHIMADZU spectrofluorometer (RF-5301PC) with a detection limit of 0.001 ppb.

## Analysis of the isotopic composition of the groundwater

The groundwater of the Malagha karst aquifer, Qale-Tol alluvial aquifer, Chidan karst springs, and river water was collected for the analysis of stable isotopes $^2H$ and $^{18}O$. The sampling was performed in two periods: a) the dry season in July (the low groundwater level period) and the wet season in April (the high groundwater level period). The stable isotope $^{18}O$ and $^2H$ compositions of eight boreholes (SA-7, AD-201, AD-202, AD-203, AD-206, AD-207, AD-208, and AD-219), the pumping wells of the Qale-Tol alluvial aquifer ($W_1$, $W_2$, and $W_3$), the Chidan karstic springs ($S_1$, $S_5$, and $S_{12}$), and the AR at the beginning and end of the Malagha Gorge ($R_1$ and $R_2$) were measured at the Freiberg Laboratory (Technische Universität Bergakademie) using the double mass spectrometry method.

# Results

## Estimation of hydrogeological properties

The boreholes of the Malagha Aquifer and Robat Aquifer were classified into three groups based on their locations: the dam reservoir (DR) (AD-201, AD-202, AD-207, AD-210, AD-204, AD-216, and AD-206), the Malagha Gorge (MG) (AD-203, SA-16, SA-14, SA-4, SA-9, SA-7, and SAM-23) and the Robat Aquifer (RA) (AD-208, SA-11, SAM-22, SAM-21, and AD-209) (Fig. 2).

The derived permeabilities (in lugeon) from the borehole logs were classified into five groups based on the Houlsby method (Houlsby 1990): very low (0–3 lugeon), low (3–10 lugeon), moderate (10–30 lugeon), high (30–60 lugeon), and very high (more than 60 lugeon). The permeability from the top to the end of all the three DR, MG, and RA borehole groups is shown in Fig. 4. The permeability of the DR and RA boreholes was the highest while that of the MG boreholes was the lowest especially below the water table. The permeability of the MG boreholes below the water table was less than 30 lugeon (Fig. 4). The permeability of the DR boreholes was 100 lugeon for a continuous length (from 45 to 140) of the borehole.

The length and percentage of the fracture zones in all the boreholes, above and below the water table level, are shown in Fig. 5a and b, respectively. The total length of the fracture zones was about 700 m, representing 22% of the length of all the boreholes together. The fractions of the fracture zones in the DR, MG, and RA boreholes were 30%, 18%, and 15% above the water table and 21%, 9%, and 3% below the water table level, respectively (Table 1). The length and percentage of the fracture zones of the DR boreholes were higher than those of the MG and RA boreholes. Open joints are defined here as joints with an aperture of 1–10 mm. The average numbers of the open joints in 5-m intervals in the borehole log of the DR, MG, and RA were 5.6, 4.9, and 5.8, respectively, above the water table level and 5.3, 5.1, and 6.9, respectively, below the water table level (Fig. 6; Table 1). There is no significant difference between these three groups of open joints below and above the water table level. The solution cavities in the boreholes were classified into three groups: less than 1 cm, 1–5 cm, and 5–10 cm (Fig. 7). Most of the vugs had a diameter of less than 5 cm. Only a few vugs ranged from 5 to 10 cm in diameter. The MG boreholes had higher frequency vuggy zones than the DR and RA boreholes (Table 1). There was no significant difference in the number of the vugs above and below the water table level. The core washes above the water table level were in the range of zero to 10 m in each of the boreholes and were higher in the DR boreholes (Fig. 8). The core wash length
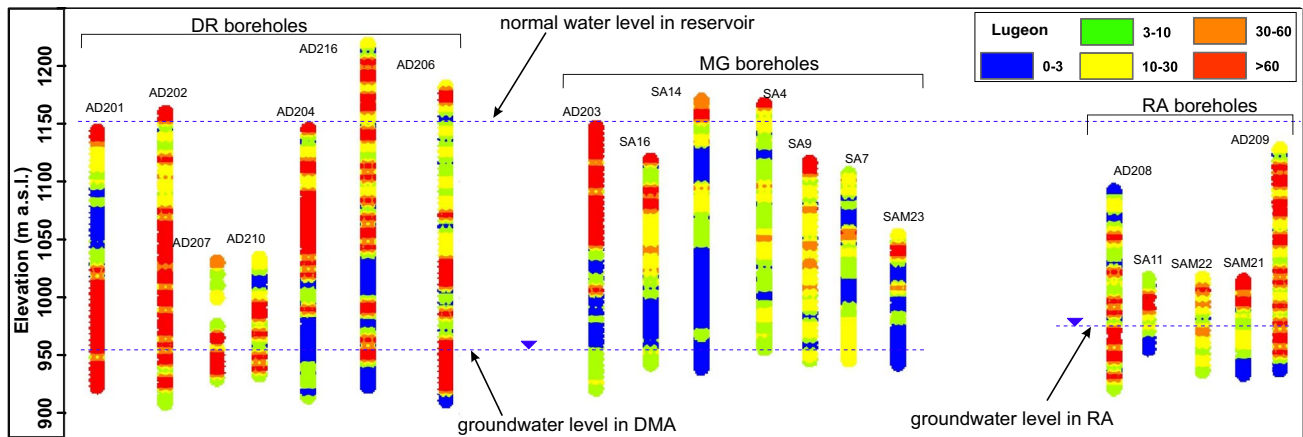
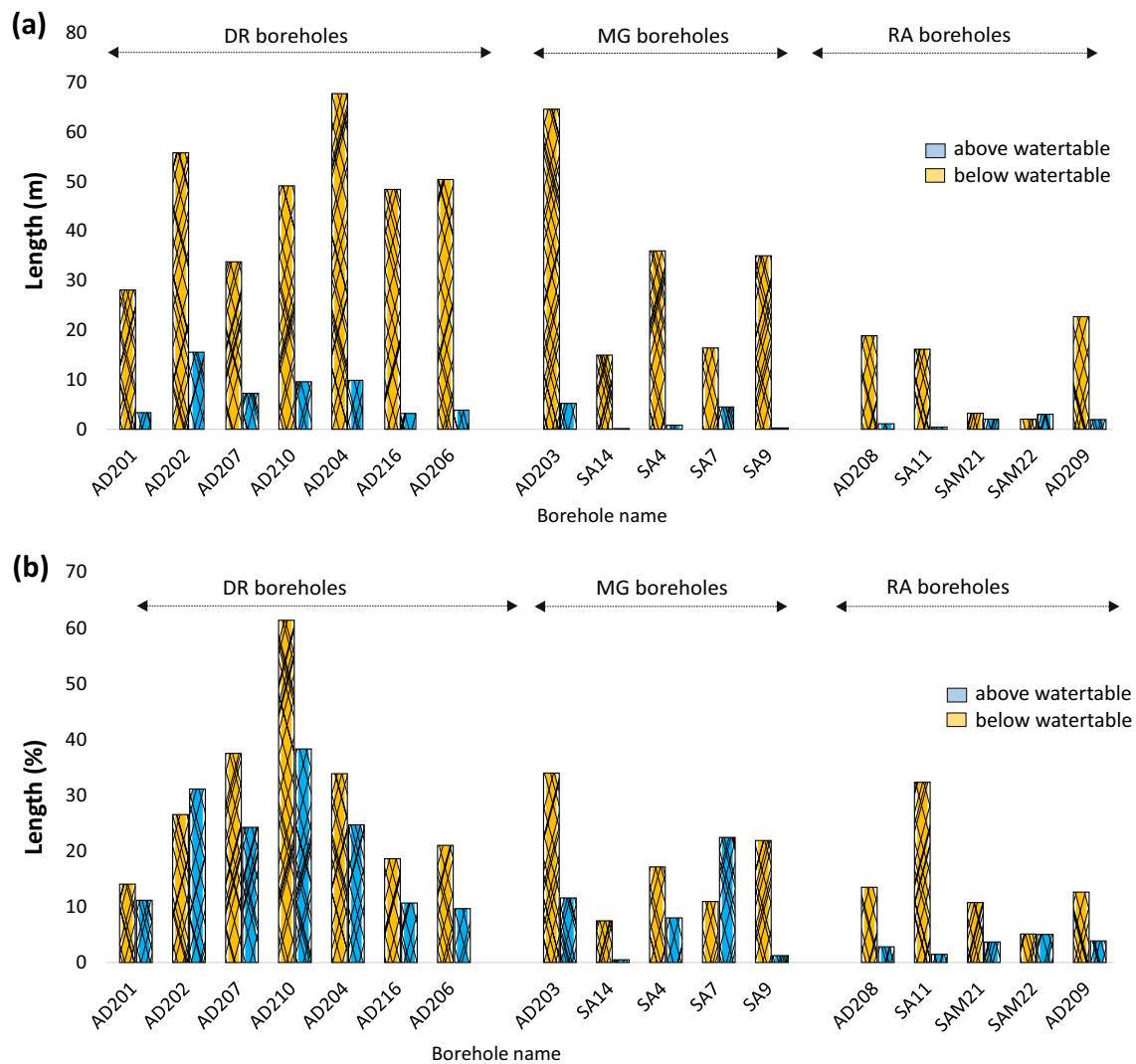**Fig. 4** The permeability (lugeon) classes of DR, MG, and RA boreholes



**Fig. 5** The length (**a**) and percentage (**b**) of the fracture zones in DR, MG, and RA boreholes above (yellow) and below (blue) the water table level

**Table 1** The average of the measurements of the abundance of the open joints, vuggy zones, fracture zones, core washes, and rod falls at DR, MG, and RA boreholes (*AWT* above water table, *BWT* below water table

| Borehole Group | Open joint[1a] | | Vuggy zone[a] | | Fracture zone[b] | | Core wash[b] | | Rod fall[c] | |
|---|---|---|---|---|---|---|---|---|---|---|
| | AWT | BWT | AWT | BWT | AWT | BWT | AWT | BWT | AWT | BWT |
| DR | 5.3 | 5.6 | 1 | 1 | 30 | 21 | 0.24 | 0.04 | 6.8 | 0.0 |
| MG | 5.1 | 4.9 | 2 | 3 | 18 | 9.0 | 0.01 | 0.00 | 0.0 | 0.0 |
| RA | 6.9 | 5.8 | 1 | 1 | 15 | 3.0 | 0.01 | 0.00 | 0.0 | 0.0 |

[a]No. per 5-m interval; [b]percentage of average length per total borehole length; [c]total length in all of the boreholes

**Fig. 6** Open joints in the DR, MG, and RA boreholes above (yellow color) and below (blue color) the water table level
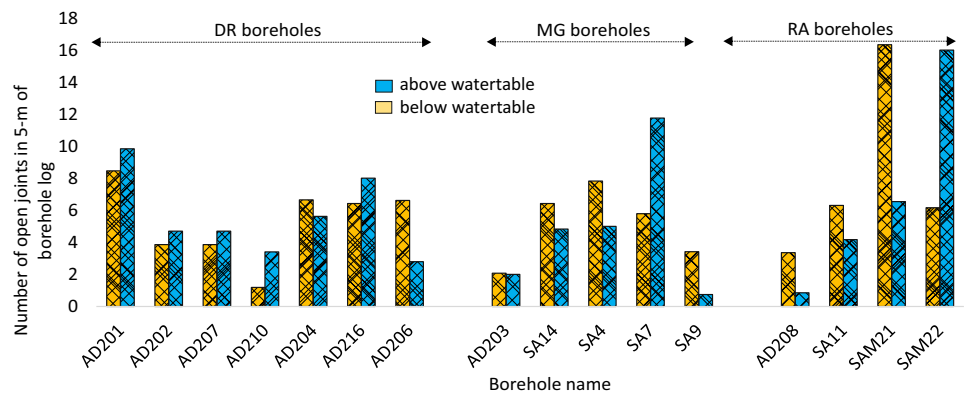


**Fig. 7** The number of vugs in the borehole logs inside DR, MG, and RA boreholes
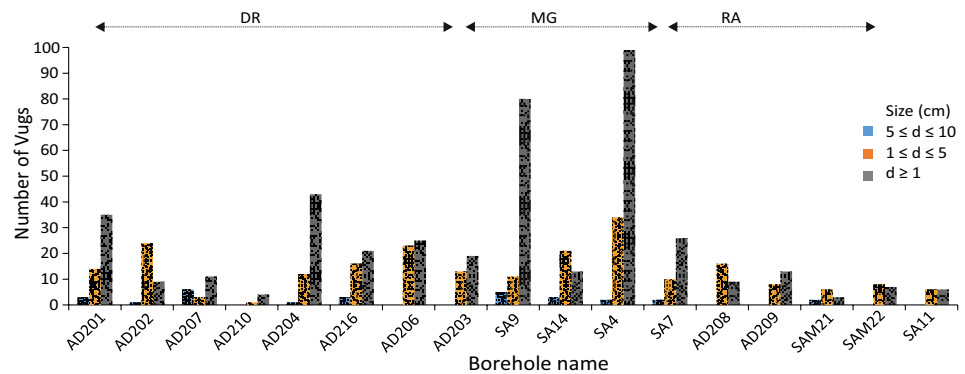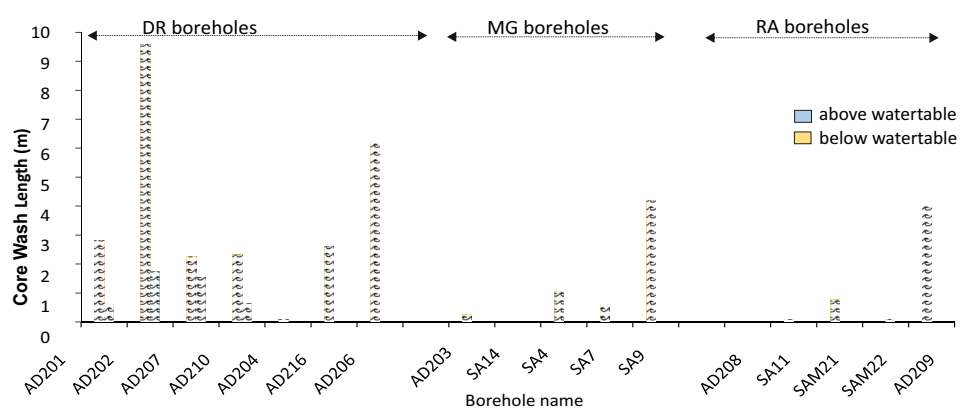


**Fig. 8** The core wash length in DR, MG, and RA boreholes above (yellow) and below (blue) the water table levels

below the water table level was less than 2 m in four DR boreholes. In the rest of the boreholes, no core wash was observed (Table 1). Rod fall was not reported neither in any of the boreholes of RA and MG nor below the water table level of the DR boreholes. Rod fall was found above the water table level in the DR boreholes: AD-202 in one section with a length of 80 cm, AD-206 in two sections with the lengths of 70 and 320 cm, AD-207 in one section with a length of 35 cm, and AD-216 in two sections with the lengths of 20 and 155 cm. The total rod fall length was 6.80 m of which 6.25 m was due to core wash. The core wash occurred in fracture zones and/or marly limestone. The 0.35 m rod fall of borehole AD-207 occurred at the contact of the fractured limestone and marlstone. The 0.20 m rod fall in borehole AD-216 seemed to be a cavity because it was located in the limestone without any fracture zones.

## Analysis of the spatial distribution of water table levels

The water table levels of all the boreholes at different times are presented in Fig. 9. Based on their water table levels, the boreholes can be divided into DMA and RA groups. The groundwater level at the dam site was about 60–70 m lower than that of the river bed (Adinehvand and Raeisi 2018). The water table levels in the RA boreholes were about 10–30 m higher than those of the DR and MG boreholes.

The Qale-Tol Fault acts as an impermeable barrier and separates the RA boreholes from the DMA boreholes (Adinehvand and Raeisi 2018). The water table level in the DMA was flat within an area of 2500 m by 900 m at any specific time (Fig. 9). The water balance showed that the main source of the DMA karst groundwater is recharge from precipitation though the Abolabbas River seepage along with the MG also has a contribution (Adinehvand and Raeisi 2018). At any specific time, the water table levels in the

boreholes close to the river (SA-7, SA-4, and AD-210) were slightly higher than those away from the river. The mound below the Abolabbas River slightly increases the water table level in the boreholes near the river (Adinehvand and Raeisi 2018).

## Analysis of the isotopic composition of the groundwater

The water samples in the dry and wet seasons can be divided into three distinct groups on the $^2$H and $^{18}$O diagram (Fig. 10). Group A consists of the water samples of the Abolabbas River ($R_1$ and $R_2$), some of the karst waters of the DMA boreholes close to the Abolabbas River, and the Chidan springs ($S_1$, $S_5$, and $S_{12}$). The water samples are most depleted in $^2$H and $^{18}$O. Group C consists of the boreholes of the Malagha Aquifer including AD-201, AD-202, AD-203, AD-206, AD-207, and AD-219 with the most enriched water samples. Group B consists of the $W_1$, $W_2$, and $W_3$ pumping wells of the Qale-Tol alluvial aquifer. This group is located between Groups A and B along the local meteoric water line (LMWL) (Fig. 10).

## Artificial dye tracer tests

The first (uranine), second (uranine), and third (rhodamine WT) tracers were injected into boreholes AD-207, AD-202, and AD-210, respectively (Fig. 2). In the first dye tracer test, the uranine dye was not detected in any sampling points during 7 months of the sampling period. According to the dye breakthrough curve of injection borehole AD-207, the dye was not trapped around the borehole intersecting the As1 Unit below the water table level (Fig. 11).

The maximum dye concentration in the injection borehole was about 1300 ppb and was reduced to 60 ppb after about 60 days from the injection time and remained constant for 280 days in the second tracer test (Fig. 12). The uranine dye

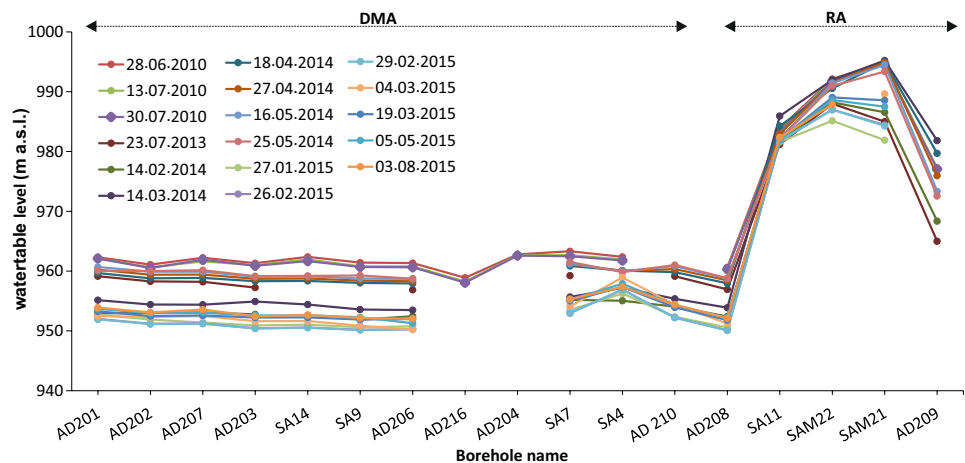**Fig. 9** The water table levels in the boreholes of DMA and RA

**Fig. 10** The $^{18}$O and $^{2}$H diagram of the water samples in the study area (GMWL: Global Meteoric Water Line; MMWL: Mediterranean Meteoric Water Line; LMWL: Local Meteoric Water Line). Chidan springs have been labeled by "S"
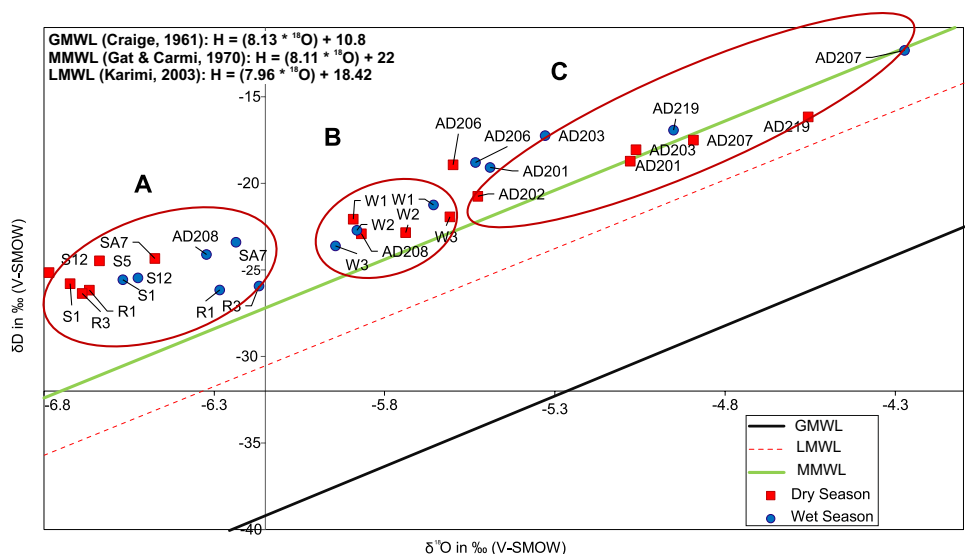


GMWL (Craige, 1961): H = (8.13 * $^{18}$O) + 10.8
MMWL (Gat & Carmi, 1970): H = (8.11 * $^{18}$O) + 22
LMWL (Karimi, 2003): H = (7.96 * $^{18}$O) + 18.42

**Fig. 11** Dye concentration in the injection borehole AD-207 in the first tracer test
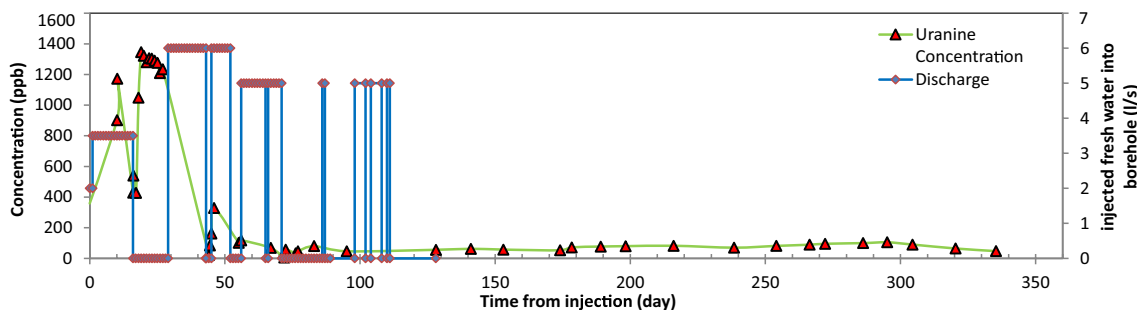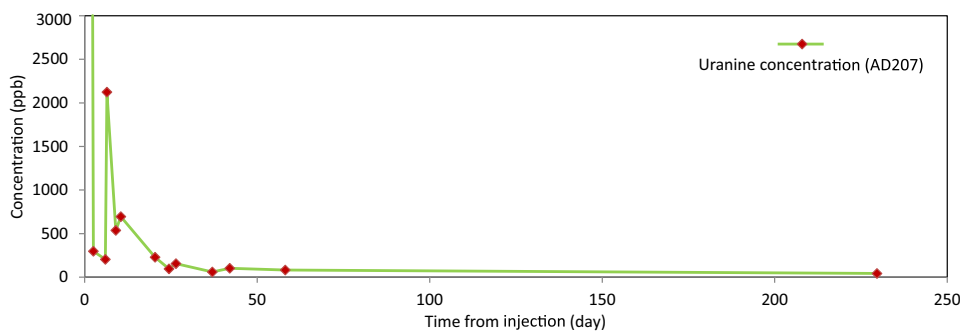




**Fig. 12 a** Daily precipitation; **b** breakthrough curve of the uranine dye in the second tracer test during the 335-day period

was only detected in the AD-207 borehole (Fig. 13). The first dye appearance was 76 days after dye injection with the dye concentration of 1.52 ppb (Fig. 13b). The breakthrough curve showed a dominant peak concentration of about 10 ppb after 235 days from the dye injection, however, it was reduced to 0.01 ppb, 25 days after the peak concentration (Fig. 13b). The horizontal distance between the injection and detection boreholes was 520 m. The dye velocities at the first dye appearance and the peak concentration were 0.40 m/h and 0.13 m/h, respectively.

In the third tracer test, the dye was detected only in borehole AD-207 about 85 m far from the injection borehole AD-210 (Fig. 14). The dye breakthrough curve in the detected borehole is shown in Fig. 15. There were not any other boreholes in the vicinity of the injection borehole especially in the west direction to detect the dye and determine the general flow direction. The breakthrough curve shows six dye peaks namely C1–C6. The concentrations of the C1–C5 dye peaks varied from 42 to 121 ppb and returned to the background concentration in a short time (Fig. 15b).
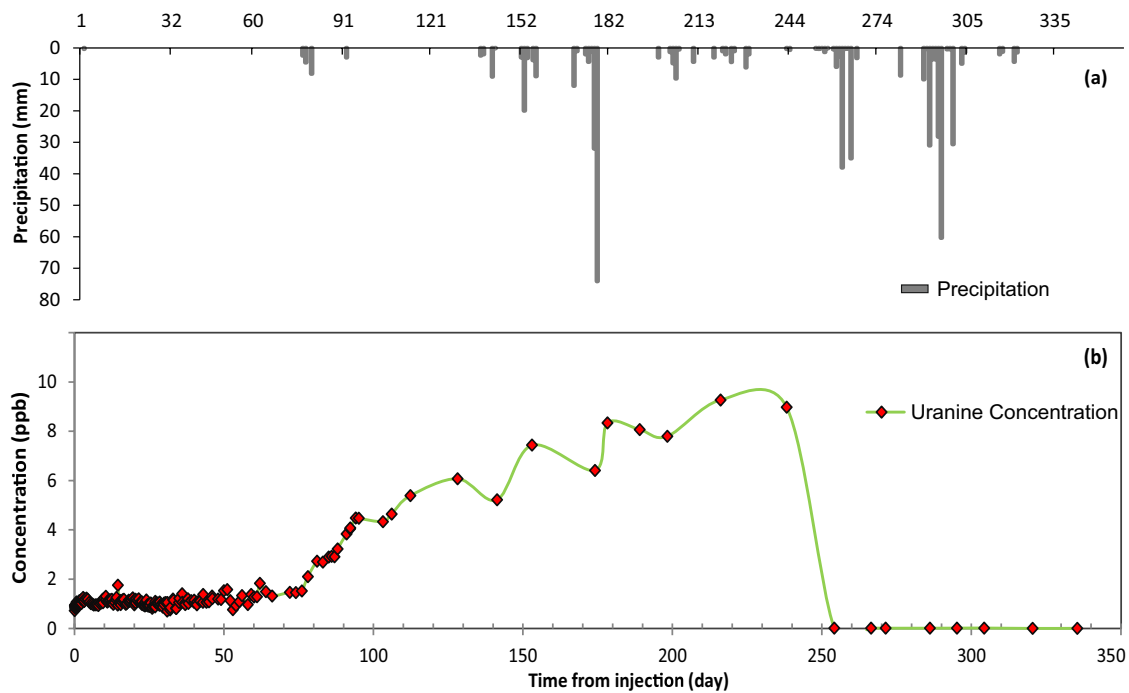
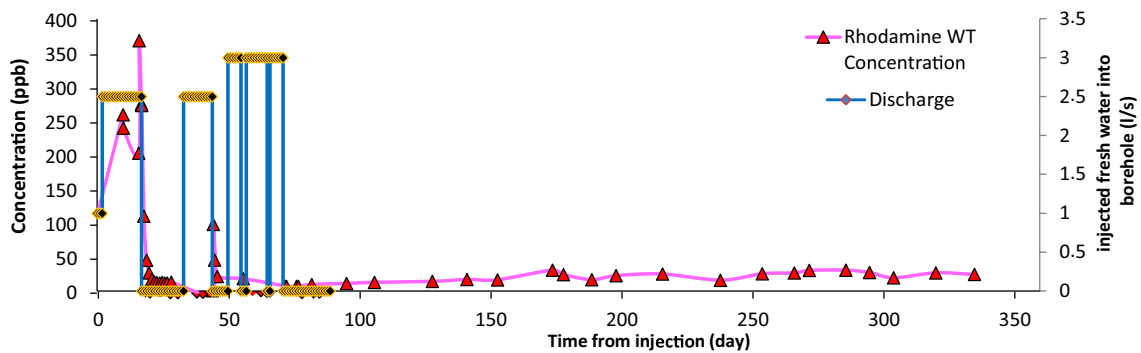**Fig. 13** Dye concentration and water injection periods in borehole AD-202 in the second tracer test



**Fig. 14** Dye concentration and water injection periods in the injection borehole AD-210 in the third tracer test

The velocity of the first dye appearance (C0) was 0.63 m/h and the velocities of the C1 to C6 peaks varied from 0.30 to 0.04 m/h (Table 2).

## Discussion

### Hydrogeological properties

Characterization of the Malagha Aquifer was performed based on the borehole logs, significantly fractured and crushed zones (Fig. 5), numerous open joints (Fig. 6), core washes in most of the boreholes (Fig. 8), solution cavities of mainly less than 1 cm and no cavities of bigger than 10 cm

(Fig. 7), and continuous high permeabilities of 100 lugeon up to 140 m of the borehole length (Fig. 4). Adinehvand and Raeisi (2018) showed that the DMA and RA are located in the damage zone of the Qale-Tol and Malagha thrust faults. The activity of these two thrust faults has resulted in extensive joints, fracture zones, and minor faults (Adinehvand and Raeisi 2018). A large number of fracture zones and densely fractured limestone act as transmissive zones and impede the formation of conduits in the system. High and continuous permeabilities which have a good correlation with the fracture zones prevent the formation of large conduits. This implies that the karst groundwater flows through a large volume of the rock mass instead of conduits. The opening with an aperture of 1 cm is the threshold of the dividing fracture
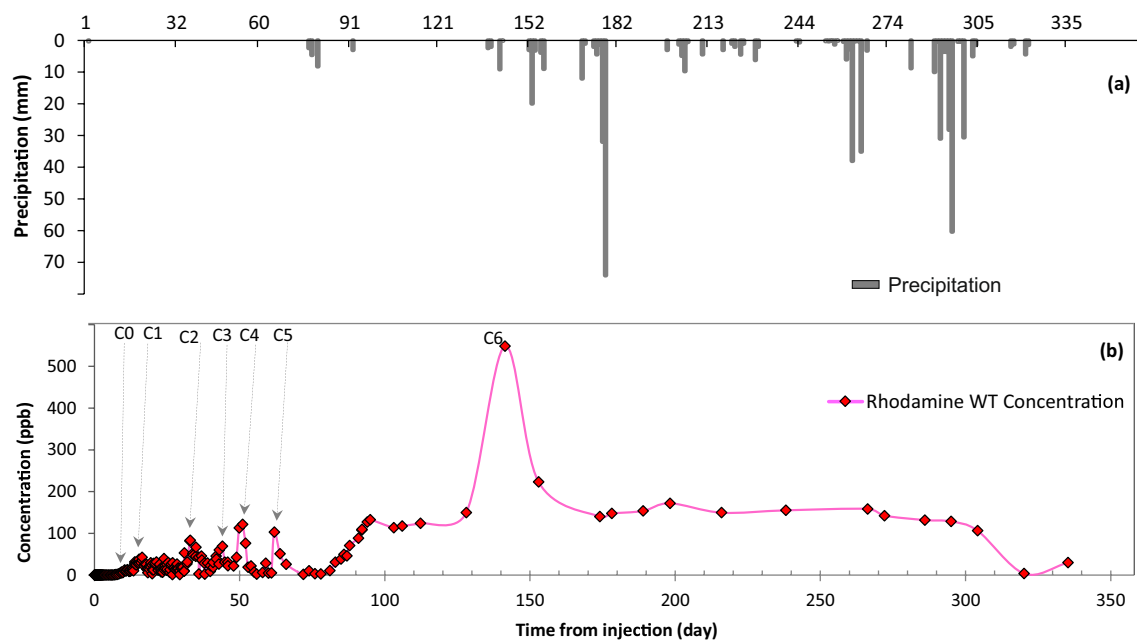
**Fig. 15** **a** Daily precipitation; **b** dye breakthrough curve of the rhodamine WT in borehole AD-207 during 335 days in the third tracer test

**Table 2** The velocities of the first dye appearance and peak concentrations between the injection and sampling points in the third tracer test

| Detection borehole | Situation | Time from injection (day) | Peak concentration (ppb) | Distance (m) | Dye velocity (m/h) |
|---|---|---|---|---|---|
| AD-207 | C0[a] | 7.9 | 1.93 | 85 | 0.63 |
| | C1 | 16.4 | 42.66 | 85 | 0.30 |
| | C2 | 32.8 | 32.82 | 85 | 0.15 |
| | C3 | 44.0 | 69.06 | 85 | 0.11 |
| | C4 | 51.0 | 121.31 | 85 | 0.10 |
| | C5 | 61.9 | 102.98 | 85 | 0.08 |
| | C6 | 141.3 | 548.31 | 85 | 0.04 |

[a]Is considered as the first dye appearance and not a peak concentration

(less than 1 cm) from the conduit (larger than 1 cm) aquifers (Field 2002; White 2002). They have an important role in water transport. The existence of numerous open joints (more than 0.1 cm and less than 1 cm aperture) indicates that the karst groundwater can flow through an extensive network of joints and openings.

The number of joints usually decreases with depth (Engelder 1987; Boutt et al. 2010) However, in the dam-site and reservoir boreholes, the number of joints does decrease with depth (Table 1 and Fig. 6). The fracture zones were observed with the same variations throughout and up to the end of all the boreholes (Fig. 5). Almost all of these boreholes were located in the damage zones of the Malagha and Qale-Tol thrust faults. The uniform distribution of the joint and fracture zone frequencies, which does not change with depth, demonstrates the role of the tectonic activities of

these faults which affected the rock mass column at greater depths. The interconnection of the solution cavities which are created by chemical dissolution can lead to a conduit flow regime (Atkinson 1977; White 2002). The variations in the cavity frequencies with depth showed that there was no significant difference in the number of cavities with depth. The existence of small vugs and the lack of large vugs with a diameter of more than 10 cm implied that karstification was not well developed. There was also a poor interdependence between permeability (Fig. 4) and the distribution of cavities which may imply that high cavity frequencies were not necessarily accompanied by high permeabilities. The core washes in the borehole logs are crushed rocks (washed out during drilling) with very fine grain sizes due to the high fracture and fault density. The large number of core washes in the boreholes (Fig. 8) as a result of high fracture

density suggests that the chance of the aquifer to form large conduits was low. The formation of a damage zone between the two thrust faults which formed a network of open joints and crush zones to the greater depths resulted in a high permeable media. Through this media, the water flows through a network of fracture and joint openings more or less alike to groundwater flow through intergranular unconsolidated materials. This corroborates previous findings that the type of flow in the DMA is mainly diffuse as previously proposed by Adinehvand and Raeisi (2018) and Adinehvand et al. (2017).

## Spatial distribution of water table levels

The DMA has been dissected by an extensive network of fractures. Therefore, the lack of the main conduits in the DMA to drain the system and/or a highly permeable system has caused the groundwater to flow through the extensive fractured media leading to an almost flat water table level and indicating a fissured karst aquifer system (Mangin 1975; El-Hakim and Bakalowicz 2007). In the boreholes drilled in the DMA and passing through the As2 Unit with an impermeable layer, no perched water table was observed and all of these boreholes showed the same water table levels in any specific time. The extensive fracturing of the aquifer media caused the marly layers of the As2 Unit not to have their impermeable function as the same water table levels can be seen in the boreholes above and below the As2 Unit (Adinehvand and Raeisi 2018).

## Artificial tracer tests

In the first tracer test, the dye was not detected in any boreholes. The dye was not trapped around the injection borehole because the dye concentration in the injection borehole was significantly reduced after a few days (Fig. 11). The lack of dye appearance in the nearby boreholes may be due to the fact that (a) there were no other boreholes in the As1 Unit (AD-210 was not constructed at the time of the second tracer test); (b) the flow regime may be diffuse, consequently, the dye was absorbed by the rock matrix; (c) the flow direction was not towards the MG and the DR boreholes.

The dye was detected only in AD-207 borehole during the second dye tracer test. The dye velocities based on the first dye appearance and peak concentration were 0.40 and 0.13 m/h, respectively. The flow type was most probably diffuse because the velocities were significantly less than the ranges reported for the conduit flow by Milanovic (1981, 7.2–1880 m/h), Ford and Williams (2007, 4.5–1450 m/h), as well as ASTM (1998), Worthington (1991), Worthington and Ford (2009), Gale (1984), and Quinlan and Ewers (1985) (more than 3.6 m/h). The mild slope of the raising limb of the breakthrough curve may also indicate a diffuse flow

regime (Mangin 1975; El-Hakim and Bakalowicz 2007). The sharp recession of the breakthrough curve may be due to dye dilution by precipitation (Fig. 13b). The decrease of dye concentration in the injection borehole from about 1300 to 60 ppb after about 60 days from dye injection and its remaining constant for a long period may indicate that the tracer did not remain around the injection borehole (Fig. 13).

The low hydraulic gradient caused extreme dispersivity. The dye most probably flowed in the dip direction and then in the direction parallel to the strata's strikes before being finally detected in AD-207 borehole. The dye did not appear in the MG boreholes. The main reasons were probably the low permeability and the fact that the mound was below the Abolabbas River bed in this direction. The dye flow path changed parallel to the strata's strikes near the contact of the Pabdeh-Gurpi marls and As1 Unit below the Abolabbas River bed, where the river flows on the impermeable Pabdeh-Gurpi marls and there is no mound below the river bed. The karst groundwater most probably reaches the Qale-Tol alluvial aquifer (Adinehvand and Raeisi 2018). The lack of dye appearance in the Qale-Tol exploitation wells may be due to the high dye absorption by the diffuse flow system in karst and alluvium, dilution, and decay due to the long residence time. The dye passed through the As2 Unit in spite of 21 m of marly layers because the permeabilities of the As2 Unit are high due to faulting and fracturing which allow flow across stratification (Goldscheider and Drew 2007). In addition, no perched water table was observed above this unit in several boreholes intersecting with the As2 Unit.

Similar to the second tracer test, the results of the third tracer test indicate that the flow regime was diffuse. The first five dye peaks were most probably under the effect of the high water table in the injection borehole (Fig. 15b). The breakthrough curve had a long and plateau-like shape for 212 days with a persistent tracer concentration of about 130 ppb, except for a sharp peak with the concentration of 548 ppb. The unexpected peak may be due to a preferential flow path and merits more research. There was no borehole in the direction towards the Qale-Tol aquifer to detect the dye. The dye spread inside the aquifer by the diffusion process and was detected in borehole AD-207. The diffusion process was confirmed for the following reasons: (a) the groundwater had a low hydraulic gradient; (b) the small multi-peak of the rhodamine WT breakthrough curve was directly linked to the freshwater injected into the injection borehole and the peaks returned to the background concentration after the injection of freshwater was stopped; (c) the long plateau-like breakthrough curve revealed that the dye was stored in an extensive area by diffusion and gradually passed through the media and was finally detected in borehole AD-207. The three small peaks on the rising limb of the breakthrough curve may be due to precipitation or on/off periods of freshwater injection into the borehole (Figs. 12,

13a). The breakthrough curves of uranine and rhodamine WT showed that the Malagha karst aquifer was not a fast-flushing system. A similar behavior has been observed in artesian (Goldscheider 2008) and also in unconfined shallow (Goldscheider 2005b) alpine karst aquifers. The diffuse flow regime and the lack of the main conduits in the DMA are also compatible with the results of a previous modeling study at the dam site by Adinehvand et al., (2017).

## General flow direction and leakage routes from the dam reservoir

The two alternative flow paths of the DMA karst groundwater are towards the Chidan Anticline and the Qale-Tol alluvial aquifer (Fig. 16a). The general flow direction was towards the Qale-Tol alluvial aquifer based on the following reasons: (a) the flow direction in the second dye tracer test showed the general flow direction; (b) the stable isotopes $^{18}$O and $^{2}$H of the Qale-Tol pumping wells (B Group) had mixed compositions from the Abolabbas River water (A Group) and the Malagha Aquifer (C Group) (Fig. 10); (c) the hydraulic gradient towards the Qale-Tol alluvial aquifer was much steeper than that towards the Chidan springs (Adinehvand 2017); (d) the impermeable core of the Qale-Tol thrust fault impeded the flow perpendicular to the fault which was confirmed by the water table level differences on both sides of the fault core (Fig. 16a) (Adinehvand and Raeisi 2018).

According to previous findings, after dam impoundment and the increasing of the pressure head in the dam reservoir, there will be three possible leakage routes from the dam reservoir based on the identified geological and hydrogeological settings (routes I, II, and III in Fig. 16b, c). The first leakage route (route I) will be along the bedding planes and in the direction of the general flow direction before dam construction (Fig. 16a, b). In the second leakage route (route II), the water will leak from the dam reservoir and will flow perpendicular to the bedding planes in the DMA passing through the Robat Anticline. Finally, it will emerge from the springs of the northern-limb of the Chidan Anticline (Fig. 16b, c). In the third route (route III), leaked water from the dam reservoir will pass through the dam abutments and foundation and after a short path will discharge to the Abolabbas River in the downstream (Fig. 16b, c). The leakage water will not discharge into the Abolabbas River in the downstream (Fig. 16b, c) until the water table level inside the DMA rises about 60 m and reach the riverbed elevation. As discussed above, the most probable leakage route will be towards the Qale-Tol alluvial aquifer, 11 km away from the dam site (Fig. 16a). The leakage will be controlled by the total head loss from the dam reservoir to the Qale-Tol alluvial aquifer. Therefore, the leakage will significantly decrease under long-distance flow paths and especially under the laminar flow regime in the DMA. The leakage

in this route will extensively increase because of the short leakage route with a high head loss (route II in Fig. 16b, c).

## Implications for dam construction and grout curtain layout

Several alternatives have been suggested for the grout curtain layout. One of these alternatives is to extend a two-row hanging grout curtain laterally from both sides of the dam site to the impermeable Pabdeh-Gurpi marls. For this layout, the length of the grout curtain on the right and left abutments will be 650 and 750 m, respectively with a depth of 213 m (Fig. 17). Drainage galleries will be placed downstream of the grout curtain to drain the leaked water (Fig. 17). The grout curtain of the right abutment will be connected laterally to the nearby impermeable Pabdeh-Gurpi marls. In the left abutment, the grout curtain must be laterally extended to 1500 m to be connected with the impermeable Pabdeh-Gurpi marls (see Fig. 2). The dimensions of the grout curtain will be modified after extensive data collection and detailed studies (Mahab Ghodss Consulting Engineers 2012). The bottom elevation of the grout curtain below the dam foundation and both abutments will be about 880 and 950 m a.s.l., respectively (Fig. 17). The grout curtain will be hanging because the depth of the karstic Asmari Limestone cannot be exactly determined and may be more than 600 m due to the overthrusting and repetition of the Asmari Limestone strata. In addition, the local base of erosion is about 850 m a.s.l. in the adjacent alluvial aquifer.

According to the hydrogeological characterization of the previous sections, the type of flow in the DMA was diffuse because: (a) the dye velocity was significantly less than the ranges reported for the conduit flow; (b) numerous open joints, fracture zones, lack of large solution cavities, and high and continuous permeabilities confirmed the diffuse flow regime; (c) a process-based semi-distributed model to simulate the behavior of DMA showed that the system's hydrodynamics can be well reflected when the conduit flow around the dam site is omitted (Adinehvand et al. 2017); (d) the DMA karstic aquifer had an alluvial-like behavior which was not similar to that of a typical karst aquifer (Adinehvand and Raeisi 2018). In spite of the diffuse flow, the construction of the grout curtain will be inevitable due to these reasons: (1) the extensive crushed zones in most of the boreholes are stable under the present groundwater level and hydraulic gradients, however, it is very likely that they will be unstable and washed out under high hydraulic gradients after dam impoundment. Washout has been reported in most of the boreholes (Fig. 8). Milanovic (2005) stated that the registered breccia zones (consisting of a sandy clay matrix) with a thickness of between 5 and 10 m in the Abolabbas Dam site are very weak and weathering-prone. (2) Inside the dam reservoir, for a continuous length of 45–140 m of
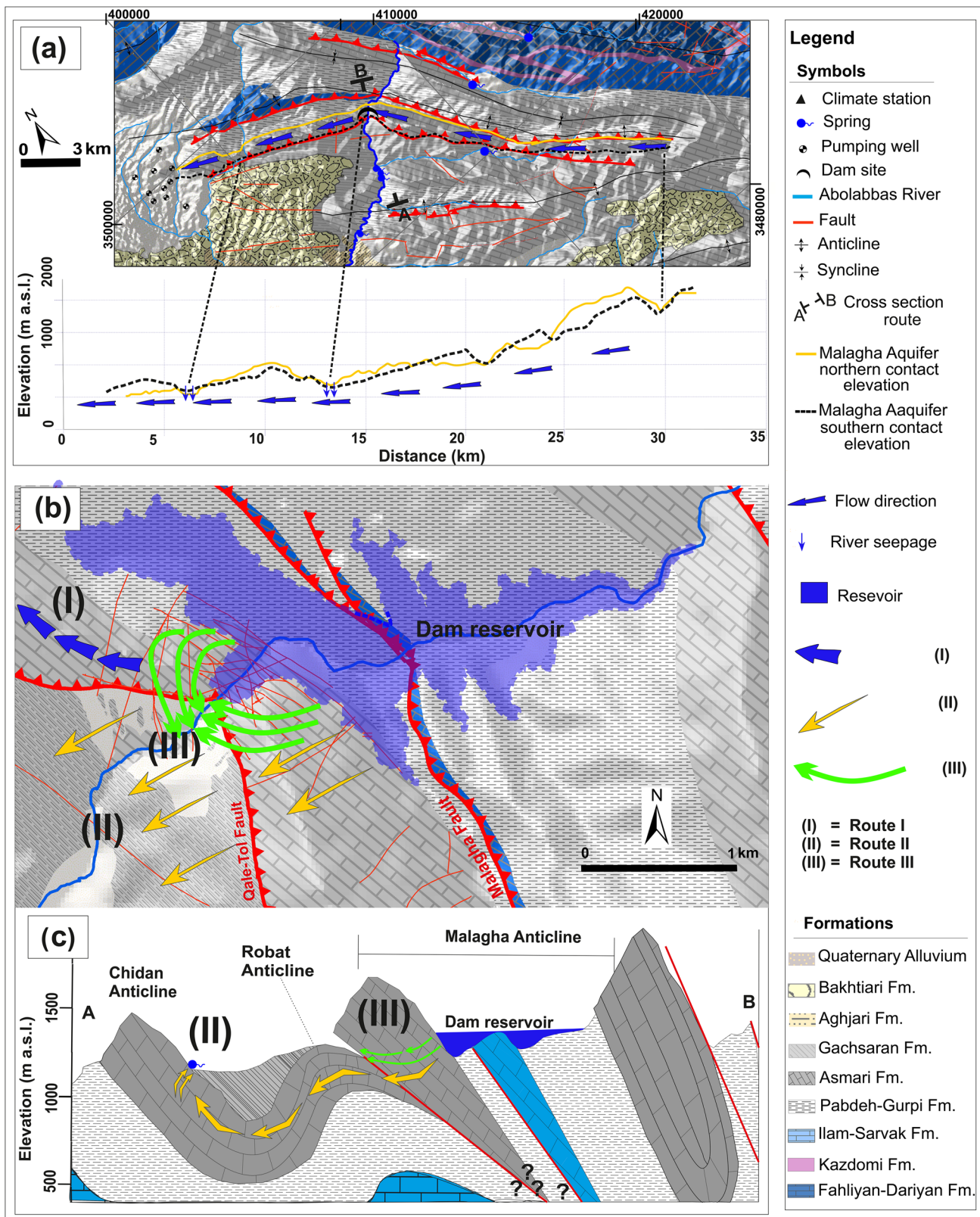
**Fig. 16** The schematic representations of the proposed models of the general flow direction (**a**) before dam construction (the contact elevation topography is also depicted in the lower figure); **b** and **c** show three alternative leakage routes after dam impoundment
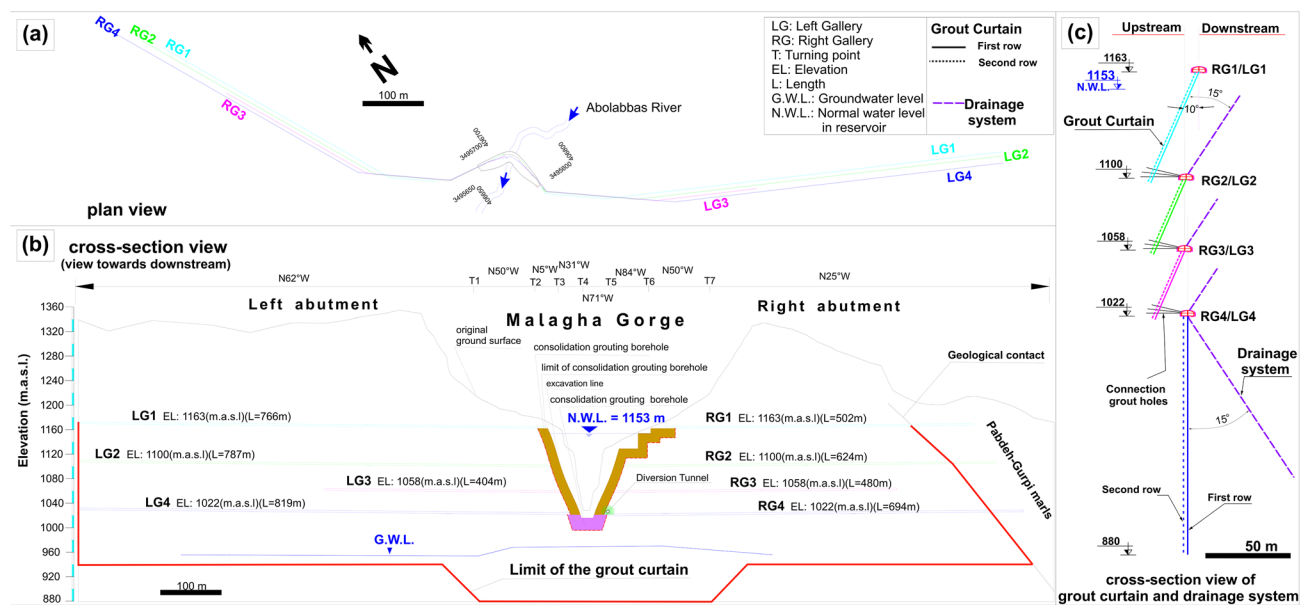
**Fig. 17** The Grout curtain layout at the Abolabbas Dam site; **a** plan view of grouting borehoes; **b** a cross-section through the Malagha Gorge and limites of the grout curtain; **c** a cross-section representing grout curatain and drainage system

the rock mass column, the permeabilities were 100 lugeon (Fig. 4). The minimum elevation of the bottom of the boreholes was about 910 m a.s.l. and the permeabilities up to 100 lugeon observed at the bottom of the boreholes implied that the permeability may also be high at greater depths. The extensive area of high permeabilities may result in a huge leakage. (3) The leakage length (the contact of the reservoir water level with bare limestone) will be about 2500 m (Figs. 2, 16b). The minimum peak velocity calculated by two tracer tests was 0.04 m/h. Without a grout curtain, the leakage through a cross-sectional area of 500,000 m$^2$ (2500*200 m) will be about 504 Mm$^3$ per year under a very small hydraulic gradient at the present time and it will be much higher with a water head of 200 m in the filled reservoir. Therefore, the leakage will most probably be extensive even under a diffuse flow regime. (4) Although most of the parameters are in favor of a diffuse flow regime, a conduit system which has not been detected by any of the boreholes yet may be located above the water table. The tracer tests represent the properties of the aquifer only below (and not above) the water table level. (5) The total average inlet water to the dam reservoir is about 3 m$^3$/s, therefore, a leakage of 1 m$^3$/s will result in dam failure.

The grout curtain must be connected to the underlying impermeable formation or the base of karstification. The bottom elevation of the overturned Asmari Limestone in the DMA or, in other words, the depth of the impermeable bedrock is unknown since no boreholes intersect with the impermeable Pabdeh-Gurpi marls. Because of overthrusting which results in the double thickening of the Asmari

Limestone at the dam site, connecting the grout curtain to the impermeable layer is not possible with the present technology. Consequently, the only possible solution is connecting the grout curtain to the base level of karstification. The permeability at the end of some of the deepest boreholes (AD-202 and AD-206) is around 100 lugeon which may indicate that the base of karstification is below 910 m a.s.l. In karst regions, the long distances and the steep dip slope of strata as in the Malagha Aquifer lead to higher groundwater flow-depths as mentioned by Worthington (2001). The water table level in the Qale-Tol alluvial aquifer which is about 850 m a.s.l. (Adinehvand et al. 2017) can be regarded as the approximate base level of karstification, which should be verified by drilling new deep boreholes along with the grout curtain. The final decision on the grout curtain layout depends on further hydrogeological information and the cost of the grout curtain.

## Conclusions

In this study, the information contained in the stable isotope data, water table levels, and tracer tests were analyzed to evaluate the leakage potential of the DMA. In addition, the data of fracture zones, open joints, permeability, solution cavities, core washes, and rod falls in the borehole logs were collected and analyzed. These analyses were applied as an integrated approach for the characterization of the Malagha karst aquifer in a rough topography and a highly tectonized zone. The tectonic activities of the thrust

faults which affected the Malagha Aquifer appeared in the form of extensive fracture zones, continuous high permeabilities with a great length, small-sized solution cavities, numerous open joints, and loose materials of the crashed zones in the boreholes. Due to these faults, the lithologically impermeable marly layers of the As2 Unit lost their role as flow barriers. The irregular and uneven water levels in the DMA with low groundwater level variations in any specific time and tracer tests demonstrated a diffuse flow regime. Using the integration of different data and approaches including geological settings, water balance, dye tracers, stable isotopes, the hydraulic gradient, and the impermeable core of the Qale-Tol thrust fault led to the conclusion that the general flow direction is parallel to the fault plane along the strike towards the Qale-Tol alluvial aquifer in the downstream.

After dam impoundment, the bare and highly permeable limestone will be in direct contact with the dam reservoir which will thus cause a huge leakage. In spite of the diffuse flow regime, the vast area of the highly fractured bare limestone will probably lead to a huge leakage. Concerns about the loose materials of the crashed zones are serious since they will probably be washed out and, consequently, a huge leakage may occur under the high hydraulic gradients. The hanging river bed and the unknown impermeable layer depth will make decision-making about designing a suitable grout curtain more complicated. The overall conditions suggest that the grout curtain must be extended to the lower levels of the base of karstification vertically and to the impermeable layer laterally.

The geology and hydrogeology of karst aquifers in highland tectonized zones are different from those in simply folded structures. Integrating different approaches in this study has significantly improved the characterization of karstic aquifers in highland tectonized zones and decision-making on the water tightening of water structures. Although this study was a local-scale characterization and the karst is site-specific, the approaches and findings of this study can be useful in studying other karst aquifers with regard to water structures in rough and tectonized regions where there is little information about karst systems.

# References

Adinehvand R (2017) Evaluation of water leakage potential from abolabbas karst dam site using hydrogeology, modeling and dye tracing methods [Ph.D. dissertation]. Shiraz, University of Shiraz

Adinehvand R, Raeisi E (2018) Characterization of a karst aquifer in a complex tectonic region, Southwestern Iran. J Cave Karst Stud 80:190–205. https://doi.org/10.4311/2017ES0107

Adinehvand R, Raeisi E, Hartmann A (2017) A step-wise semi-distributed simulation approach to characterize a karst aquifer and to support dam construction in a data-scarce environment. J Hydrol 554:470–481. https://doi.org/10.1016/j.jhydrol.2017.08.056

Alavi M (2004) Regional stratigraphy of the Zagros fold-thrust belt of Iran and its proforeland evolution. Am J Sci 304:1–20. https://doi.org/10.2475/ajs.304.1.1

Asadi N (1998) Investigation of water leakage problems from Tangab Dam site using dye tracer tests [Ms. thesis]. Shiraz University, (in Farsi)

Ashjari J, Raeisi E (2006) Influences of anticlinal structure on regional flow, Zagros. Iran J Cave Karst Stud 68:118–129

ASTM (1998) D 5717—95, Standard guide for design of ground-water monitoring systems in karst and fractured-rock aquifers: annual book of ASTM standards

Atkinson TC (1977) Diffuse flow and conduit flow in limestone terrain in the Mendip Hills, Somerset (Great Britain). J Hydrol 35:93–110. https://doi.org/10.1016/0022-1694(77)90079-8

Bagheri R (2007) Water leakage potential from Seymareh Dam site [Ms. thesis]. Shiraz University, (in Farsi)

Bakalowicz M (2005) Karst groundwater: a challenge for new resources. Hydrogeol J 13:148–160. https://doi.org/10.1007/s10040-004-0402-9

Bedmar AP, Araguas L (2002) Detection and the prevention of leaks from dams. CRC Press, Boca Raton

Berberian M (1995) Master "blind" thrust faults hidden under the Zagros folds: active basement tectonics and surface morphotectonics. Tectonophysics 241:193–224. https://doi.org/10.1016/0040-1951(94)00185-C

Berberian M, King GCP (1981) Towards a paleogeography and tectonic evolution of Iran: reply. Can J Earth Sci 18:1764–1766. https://doi.org/10.1139/e81-163

Blanc EJ-P, Allen MB, Hassani H et al (2003) Structural styles in the Zagros simple folded zone, Iran (Abstract). AAPG Int Conf 3:90017. https://doi.org/10.1144/0016-764902-110

Boutt DF, Diggins P, Mabee S (2010) A field study (Massachusetts, USA) of the factors controlling the depth of groundwater flow systems in crystalline fractured-rock terrain. Hydrogeol J 18:1839–1854. https://doi.org/10.1007/s10040-010-0640-y

Bozovic A, Budanur H, Nonveiller E, Pavlin B (1981) The Keban dam foundation on karstified limestone—A case history. Bull Int Assoc Eng Geol Bulletin de l'Association Internationale de Géologie de l'Ingénieur 24:45–51

Bruce DA (2013) Design, construction and performance of seepage barriers for dams on carbonate foundations. Carbonates Evaporites 28:229–241. https://doi.org/10.1007/s13146-012-0095-4

Craig H (1961) Isotopic variations in meteoric waters. Science 133:1702–1703. https://doi.org/10.1126/science.133.3465.1702

De Waele J (2008) Interaction between a dam site and karst springs: the case of Supramonte (Central-East Sardinia, Italy). Eng Geol 99:128–137

El-Hakim M, Bakalowicz M (2007) Significance and origin of very large regulating power of some karst aquifers in the Middle East. Implication on karst aquifer classification. J Hydrol 333:329–339. https://doi.org/10.1016/j.jhydrol.2006.09.003

Engelder T (1987) Joints and shear fractures in rock. In: Atkinson BK (ed) Fracture mechanics of rock. Academic Press, Cambridge, pp 27–69

Falcon NL (1974) Southern Iran: Zagros mountains. Geol Soc London Spec Publ 4:199–211. https://doi.org/10.1144/GSL.SP.2005.004.01.11

Field M (2002) The QTRACER2 Program for tracer-breakthrough curve analysis for tracer tests in karstic aquifers and other hydrologic systems

Ford DC, Williams PD (2007) Karst hydrogeology and geomorphology. Wiley, Hoboken

Gale SJ (1984) Quaternary hydrological development in the Morecambe Bay karst, northwest England. Nor Geogr Tidsskr Nor J Geogr 38:185–192. https://doi.org/10.1080/00291958408552124

Gat JR, Carmi I (1970) Evolution of the isotopic composition of atmospheric waters in the Mediterranean Sea area. J Geophys Res 75:3039–3048

Ghobadi MH, Khanlari GR, Djalaly H (2005) Seepage problems in the right abutment of the Shahid Abbaspour dam, southern Iran. Eng Geol 82:119–126

Goldscheider N (2005a) Karst groundwater vulnerability mapping: application of a new method in the Swabian Alb, Germany. Hydrogeol J 13:555–564. https://doi.org/10.1007/s10040-003-0291-3

Goldscheider N (2005b) Fold structure and underground drainage pattern in the alpine karst system Hochifen-Gottesacker. Eclogae Geol Helv 98:1–17. https://doi.org/10.1007/s00015-005-1143-z

Goldscheider N (2008) A new quantitative interpretation of the long-tail and plateau-like breakthrough curves from tracer tests in the artesian karst aquifer of Stuttgart, Germany. Hydrogeol J 16:1311–1317. https://doi.org/10.1007/s10040-008-0307-0

Goldscheider N, Drew D (2007) Methods in karst hydrogeology: IAH: international contributions to hydrogeology, vol 26. Taylor & Francis, Cambridge

Gutiérrez F, Parise M, De Waele J, Jourde H (2014) A review on natural and human-induced geohazards and impacts in karst. Earth Sci Rev 138:61–88. https://doi.org/10.1016/j.earscirev.2014.08.002

Hartmann A, Baker A (2017) Modelling karst vadose zone hydrology and its relevance for paleoclimate reconstruction. Earth Sci Rev 172:178–192. https://doi.org/10.1016/j.earscirev.2017.08.001

Hartmann A, Goldscheider N, Wagener T et al (2014a) Karst water resources in a changing world: review of hydrological modeling approaches. Rev Geophys 52:218–242. https://doi.org/10.1002/2013RG000443

Hartmann A, Mudarra M, Andreo B et al (2014b) Modeling spatiotemporal impacts of hydroclimatic extremes on groundwater recharge at a Mediterranean karst aquifer. Water Resour Res 50:6507–6521. https://doi.org/10.1002/2014WR015685

Hartmann A, Gleeson T, Rosolem R et al (2015) A large-scale simulation model to assess karstic groundwater recharge over Europe and the Mediterranean. Geosci Model Dev 8:1729–1746. https://doi.org/10.5194/gmd-8-1729-2015

Houlsby CA (1990) Construction and design of cement grouting: a guide to grouting in rock foundations. Wiley, Hoboken

James GA, Wynd JG (1965) Stratigraphic nomenclature of Iranian oil consortium agreement area. Am Assoc Pet Geol Bull 49:2182–2245

Jarvis T (2003) The money pit: karst failure of Anchor Dam, Wyoming. Evaporite karst Eng Probl US Okla Geol Surv Circ 109:271–278

Karimi H (2003) Hydrogeological behavior of Alvand karst aquifers, Kermanshah [Ph.D. dissertation]. Shiraz University

Mahab Ghodss Consulting, Engineers (2004) Climatology report, the first stage. Mahab Ghodss Consulting Engineers (in Farsi), Iran

Mahab Ghodss Consulting, Engineers (2012) Engineering geology report; the second stage. Mahab Ghodss Consulting Engineers (in Farsi), Iran

Majd A (2011) Hydrogeological and dye tracing studies of Abolabbas dam, Khuzestan [Ms. Thesis]. Shiraz University, (in Farsi)

Mangin A (1975) Contribution à l'étude hydrodynamique des aquifères karstiques [Ph.D. dissertation]. University of Dijon

McQuarrie N (2004) Crustal scale geometry of the Zagros fold–thrust belt. Iran J Struct Geol 26:519–535. https://doi.org/10.1016/j.jsg.2003.08.009

Merrit AH (1995) Geotechnical aspects of the design and construction of dams and pressure tunnels in soluble rocks. In: Beck, (Balkema) BF (ed) engineering and environmental problems in karst terrane. Proc. 5th conference, Gatlinburg. Rotterdam, pp 3–7

Milanovic PT (1981) Karst hydrogeology. Water Resources Publications, USA

Milanovic PT (2004) Water resources engineering in karst. CRC Press LLC, Boca Raton

Milanivic PT (2005) Abolabbas Dam project report. Mahab Ghodss Consulting Engineers, Tehran (unpublished report)

Milanovic P (2014) H2Karst research in limestone hydrogeology. Springer, Berlin

Milanovic S, Stevanovic Z, Jemcov I (2010) Water losses risk assessment: an example from Carpathian karst. Environ Earth Sci 60:817–827. https://doi.org/10.1007/s12665-009-0219-x

Mohammadi Z, Raeisi E, Bakalowicz M (2006) Method of leakage study at the karst dam site. A case study: Khersan 3 Dam. Iran Environ Geol 52:1053–1065. https://doi.org/10.1007/s00254-006-0545-1

Mozafari M, Raeisi E (2015) Understanding Karst leakage at the Kowsar Dam, Iran, by hydrogeological analysis. Environ Eng Geosci 21:325–339. https://doi.org/10.2113/gseegeosci.21.4.325

Mozafari M, Raeisi E (2017) Leakage paths at the Lar Dam site, Northern Iran. Q J Eng Geol Hydrogeol 50:444–453. https://doi.org/10.1144/qjegh2017-016

Mudarra M, Andreo B, Marín AI et al (2014) Combined use of natural and artificial tracers to determine the hydrogeological functioning of a karst aquifer: the Villanueva del Rosario system (Andalusia, southern Spain). Hydrogeol J 22:1027–1039. https://doi.org/10.1007/s10040-014-1117-1

Nassery H (1991) Hydrogeological studies of karst springs in the catchment area of Droodzan Dam [Ms. thesis]. Shiraz University, (in Farsi)

Parise M, Closson D, Gutiérrez F, Stevanovic Z (2015) Engineering geology for society and territory. In: Lollino G, Manconi A, Guzzetti F et al (eds) Engineering geology for society and territory: Urban Geology Sustainable Planning and Landscape Exploitation, vol 5. Springer, Cham, pp 479–482

Quinlan JF, Ewers RO (1985) Ground water flow in limestone terranes—strategy, rationale and procedure for reliable, efficient monitoring of ground water in karst areas. Proc Fifth Natl Symp Expo Aquifer Restor Gr Water Monit Worthingt OH 197–234.

Raeisi E, Kowsar N (1997) Development of Shahpour Cave, Southern Iran. Cave Karst Sci 24:27–34

Rahnemaaie M (1994) Evaluation of infiltration and runoff in the karstified carbonatic rocks [Ms. thesis]. Shiraz, University of Shiraz, (in Farsi)

Sissakian VK, Al-Ansari N, Knutsson S (2014) Karstification effect on the stability of mosul dam and its assessment, North Iraq. Engineering 06:84–92. https://doi.org/10.4236/eng.2014.62012

Stocklin J (1968) Structural historiy and tectonics of Iran: a review. Am Assoc Pet Geol Bull 52:11258–12229

Talebian M, Jackson J (2004) A reappraisal of earthquake focal mechanisms and active shortening in the Zagros mountains of Iran. Geophys J Int 156:506–526. https://doi.org/10.1111/j.1365-246X.2004.02092.x

Turkmen S, Özgüler E, Taga H, Karaogullarindan T (2002) Seepage problems in the karstic limestone foundation of the Kalecik Dam (south Turkey). Eng Geol 63:247–257

Unal B, Eren M, Yalcin MG (2007) Investigation of leakage at Ataturk dam and hydroelectric power plant by means of hydrometric measurements. Eng Geol 93:45–63

Uromeihy A (2000) The Lar Dam; an example of infrastructural development in a geologically active karstic region. J Asian Earth Sci 18:25–31

Uromeihy A, Barzegari G (2007) Evaluation and treatment of seepage problems at Chapar-Abad Dam. Iran Eng Geol 91:219–228

White WB (1969) Conceptual models for carbonate aquifers. Ground Water 7:180–186. https://doi.org/10.1111/j.1745-6584.2012.00923.x

White WB (2002) Karst hydrology: recent developments and open questions. Eng Geol 65:85–105. https://doi.org/10.1016/S0013-7952(01)00116-8

Wiesner E, Ewert F-K (2013) Resolving serious seepage through karstified limestone at the Mujib Dam, Jordan. Bull Eng Geol Environ 72:149–162. https://doi.org/10.1007/s10064-012-0452-5

Worthington SRH (1991) Karst hydrogeology of the Canadian Rocky Mountains

Worthington SRH (2001) Depth of conduit flow in unconfined carbonate aquifers. Geology 29:335–338. https://doi.org/10.1130/0091-7613(2001)?029%3c0335:DOCFIU%3e?2.0.CO

Worthington SRH, Ford DC (2009) Self-organized permeability in carbonate aquifers. Ground Water 47:326–336. https://doi.org/10.1111/j.1745-6584.2009.00551.x

Zarei H, Akhondali AM, Mohammadzadeh H et al (2014) Runoff generation processes during the wet-up phase in a semi-arid basin in Iran. Hydrol Earth Syst Sci Discuss 11:3787–3810. https://doi.org/10.5194/hessd-11-3787-2014